Recombinant Keratin-Chitosan Cryogel Decorated with Gallic Acid-Reduced Silver Nanoparticles for Wound Healing

Nanan Miao [1],*, Tao Jiang [1],*, Yuanchao Li [1], Sihong Xue[1], Shilei Hao[2], Chunli Zhou[1], Yujie Gu [1], Ran Li[1], Bo Yu[1], Xiaoqu Duan [1], Wenchao Xu[1], Rupeng Wang [1], Lei Ran [1]

[1]Department of Rheumatology and Dermatology, The Second Affiliated Hospital of Army Medical University, Chongqing, People's Republic of China; [2]College of Bioengineering, University of Chongqing, Chongqing, People's Republic of China

*These authors contributed equally to this work

Correspondence: Rupeng Wang; Lei Ran, Department of Rheumatology and Dermatology, The Second Affiliated Hospital of Army Medical University, Chongqing, 400037, People's Republic of China, Tel +86 23 68755739, Email Wrp71@tmmu.edu.cn; ranlei1010@tmmu.edu.cn

Background: Wound healing is a complex physiological process that can be roughly divided into four stages: hemostasis, inflammation, proliferation, and remodeling. Conventional wound dressings often fail to meet the diverse needs of these healing stages due to their limited functionality. Cryogels, however, possess several attractive properties, such as large, interconnected pores, good mechanical strength, and ease of modification, making them suitable for developing advanced dressings with multiple functions. In this study, we developed a multifunctional cryogel dressing, with biocompatible polysaccharides as the main component, designed to provide a breathable, moist, and antibacterial microenvironment for chronic infected wounds, thereby promoting wound healing.

Methods: Recombinant keratin 31 (RK31) was combined with chitosan (CS) to produce a CS/RK31 cryogel, referred to as CK. Gallic acid-reduced silver nanoparticles (GA/Ag NPs) were incorporated as the active antibacterial component to create the CS/K31@GA/Ag cryogel, known as CKGA. The cryogel was characterized using scanning electron microscopy (SEM) and a universal testing machine, and its biocompatibility was assessed in vitro. The dynamic hemostatic performance of the cryogel was evaluated with a rat tail amputation bleeding model. Additionally, the antibacterial effects of the cryogel against *Staphylococcus aureus* and *Escherichia coli* were tested using agar diffusion assays and turbidimetry. The antioxidant capacity of the CKGA cryogel was also measured in vitro. Finally, the cryogel's ability to promote wound healing was tested in an SD rat model of infected wounds.

Results: Characterization results showed that the CKGA cryogel features an interpenetrating porous network structure and exhibits excellent mechanical properties, with a swelling rate of up to 1800%. Both in vitro and in vivo experiments confirmed that the cryogel has good biocompatibility, effectively absorbs exudates, and rapidly stops bleeding. The addition of GA/Ag NPs provided significant antibacterial effects, achieving an inhibition rate of over 99.9% against both *S. aureus* and *E. coli*. Furthermore, CKGA cryogels demonstrated a strong scavenging capacity for ROS in a dose-dependent manner. Studies using the SD rat infected wound model showed that the cryogel effectively inhibited bacterial proliferation on wound surfaces, reduced local tissue inflammation, and promoted the healing of infected wounds.

Conclusion: The multifunctional cryogel, with its rapid hemostatic, antibacterial, and antioxidant properties, as well as its ability to promote cell proliferation, could be widely used as a wound dressing for the healing of bacterial infections.

Keywords: nanocomposite cryogel, hemostasis, antioxidant, antibacterial, wound healing

Introduction

The skin is the largest organ in the body and serves a crucial function by forming a barrier between the external environment and the internal tissues, thus preventing the invasion of harmful factors such as pathogens.[1] When the skin barrier is compromised, the risk of subcutaneous tissue infection increases, and inflammatory responses at the wound site can delay healing.[2] Patients with chronic wounds require standardized wound care, combined with active management of the underlying

Graphical Abstract

Wound healing
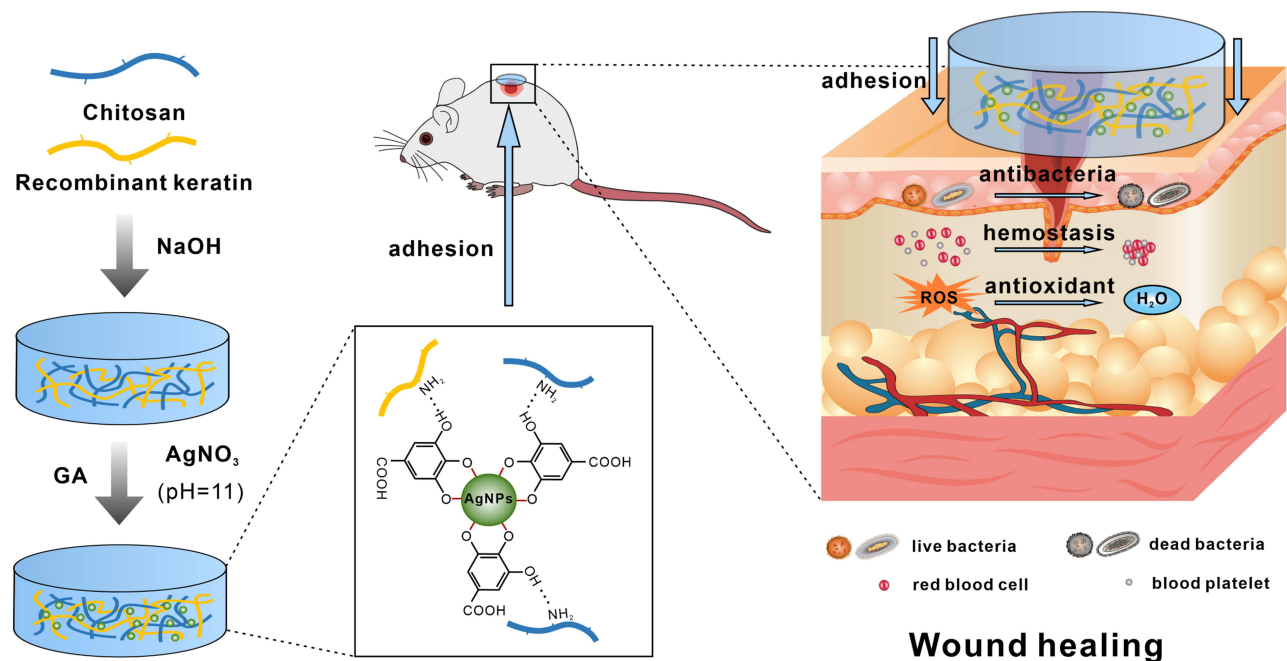
disease and its complications, leading to a significant economic burden on society and the healthcare system. According to a report from Verified Market Research®, the wound care market was valued at $201.8 billion in 2022 and is projected to reach $305.2 billion by 2030.[3] With the rising number of surgical interventions for chronic wounds, the demand for wound care products is steadily increasing. Traditional dressings, such as gauze and bandages, often provide poor isolation and can adhere to the wound, potentially causing secondary damage when changed. Improper wound care can lead to infections, and the formation of bacterial biofilms can significantly reduce the effectiveness of systemic or local antibiotic treatments.[4] Traditional dressings with antibiotics also face challenges in controlling the drug release rate, affecting therapeutic efficacy and increasing the risk of drug resistance. For deep or persistent infections, traditional dressings often fail to provide sufficient antimicrobial depth, limiting their therapeutic effectiveness.[5] In recent years, nanotechnology has demonstrated significant potential in developing antimicrobial hydrogel dressings, as well as in photodynamic and acoustic therapies.[6,7] Nanomaterials can serve as drug carriers, enabling precise drug delivery and controlled release, which effectively increases local drug concentration and enhances bactericidal effects.[8] Beyond their antibacterial properties, some innovative dressings also exhibit biological activities such as promoting cell proliferation and angiogenesis, which help accelerate the wound healing process. Consequently, traditional dressings no longer meet clinical needs, creating a demand for multifunctional dressings that can effectively block harmful substances, absorb exudate, prevent infection, maintain moisture and breathability, and promote wound repair.

Since dressings are medical products in direct contact with wounds, the biocompatibility of the synthetic materials used is crucial. Natural polymers such as keratin, chitosan, gelatin, and cellulose generally offer better biocompatibility compared to synthetic polymers such as polyacrylamide, polyethylene glycol, and polyvinyl alcohol. These natural polymers can enhance cell adhesion and tissue growth, making them promising for use in gel dressings.[9] Human hair-derived keratin, known for its low immunogenicity and excellent wound-healing properties, is commonly used in tissue engineering and regenerative medicine. Keratin can be categorized into extracted and recombinant forms. Extracted keratin's amino acid composition, molecular weight, and purity can vary due to the extraction and separation processes.[10] In contrast, recombinant keratin, produced using recombinant DNA technology, generally has higher purity and can promote epithelialization, angiogenesis, collagen deposition, and tissue remodeling during wound healing.[11] However,

recombinant keratin has poor mechanical properties, and gels formed from it may not meet clinical requirements for exudate absorption, tensile strength, or adaptability to wounds. To address this, blending recombinant keratin with other natural polymers is necessary to achieve better mechanical properties. Chitosan is a natural cationic polysaccharide known for its excellent biocompatibility. Numerous studies have shown that hydrogels made from chitosan can create a moist wound environment and enhance wound healing, particularly when combined with other polymers to boost their bioactivity.[12] In some research, chitosan was dissolved under acidic conditions, mixed with natural polymers such as keratin and gelatin, and freeze-dried to produce a loose, porous coagulum.[13,14] This method not only leverages the mechanical properties of the chitosan coagulum but also enhances its bioactivity.

However, most hydrogels made from natural polymers exhibit poor antimicrobial properties and lack resistance to bacterial infections during the wound-healing process. To address this, antimicrobial agents must be introduced into the hydrogels. Current strategies for adding antimicrobial activity involve incorporating antibiotics, antimicrobial peptides, and metal nanoparticles, with silver nanoparticles (Ag NPs) being popular due to their ease of preparation and strong antimicrobial properties.[15] Despite their success in treating infected wounds, Ag NPs face limitations such as potential accumulation at the wound site and local toxicity from direct contact with tissues.[16] Research has focused on the toxicity and mechanisms of Ag NPs in various cellular and biological models, primarily linked to oxidative stress and apoptosis.[17–19] For instance, one study using 2D keratinocytes reported increased levels of reactive oxygen species (ROS), malondialdehyde (MDA), IL-1α, IL-6, and IL-8, alongside decreased superoxide dismutase (SOD) levels, indicating that Ag NPs' cytotoxicity is associated with oxidative damage and inflammation.[20] Additional studies have noted elevated silver levels in patients' blood and skin wounds after treating burn wounds with silver sulfadiazine and nanocrystalline silver dressings.[21,22] Furthermore, the accumulation of silver nanoparticles in wounds is accompanied by slow release of silver ions, which exacerbates local tissue toxicity.[23] In recent years, many studies have reported the preparation of silver nanoparticles (Ag NPs) using plant extracts such as citric acid, tannic acid, and gallic acid (GA) as reducing agents.[24] These methods enhance the dispersion and stability of Ag NPs. Additionally, natural polyphenols can form coordination bonds with Ag NPs, creating a protective layer that reduces their cytotoxicity. GA, a natural phenolic compound, holds promise for applications in wound repair hydrogels due to its antioxidant, anti-inflammatory, and antimicrobial properties.[25] Studies indicate that under alkaline conditions, GA can reduce Ag^+ to Ag NPs, while the two phenolic hydroxyl groups on the GA molecule are oxidized to quinone forms. These quinone forms adsorb onto the surface of Ag NPs, thereby reducing their cytotoxicity.[26] Hydrogels containing GA-reduced silver nanoparticles have been reported to exhibit good biocompatibility and sustained antimicrobial activity, effectively inhibiting biofilm formation on wounds and promoting wound healing.[2,27] Therefore, this study prepared a cryogel by combining recombinant keratin 31 (RK31) with chitosan (CS) and incorporating GA-reduced Ag NPs as the active antimicrobial component. This multifunctional dressing demonstrates excellent physical properties, antimicrobial and antioxidant efficacy, promoting hemostasis and wound repair (Graphical Abstract).

Material and Methods
Materials
RK31 was obtained from Hemos Medical Biotechnology Co., Ltd. (Chongqing, China). Silver nitrate ($AgNO_3$) was sourced from Sinopharm Chemical Reagent Co., Ltd. (Shanghai, China). Gallic acid, calcium chloride ($CaCl_2$), sodium hydroxide (NaOH), glacial acetic acid (CH_3COOH), and chitosan (deacetylation degree ≥95%, viscosity 100–200 mPa·s) were purchased from Aladdin Industrial Corporation (Shanghai, China). Mouse fibroblasts (L929) cells were acquired from Senbeijia Biotechnology Co., Ltd. (Nanjing, China). *Escherichia coli* (ATCC25922) and *Staphylococcus aureus* (ATCC6538) were obtained from BeNa Culture Collection (Beijing, China). The CCK-8 kit and Calcein-AM/PI live/dead double staining kit were purchased from Solarbio Science & Technology Co., Ltd. (Beijing, China). 2′,7′-dichlorodihydrofluorescein diacetate (DCFH-DA) was obtained from Beyotime Biotechnology (Shanghai, China). The total antioxidant capacity (T-AOC) assay kit (DPPH) and total antioxidant capacity (T-AOC) assay kit (ABTS) were sourced from Sangon Biotech (Shanghai, China).

Preparation of Cryogels

After dispersing 300 mg of CS evenly in 10 mL of RK31 solution (0.4 mg·mL^{-1}), 200 μL of glacial acetic acid was added while stirring magnetically. The mixture was continuously stirred at 40°C for 6 hours to obtain a homogeneous solution. The solution was then poured into molds, and the resulting sample was freeze-dried. It was subsequently immersed in 2 mm NaOH solution for 6 hours, washed with deionized water to remove excess NaOH, and freeze-dried again to form CK cryogel. The CK cryogel was then placed in a mixed solution of GA (1 mm) and AgNO$_3$ (1 mm); the pH of the solution was adjusted to 11.0 with 1 mm NaOH, and the solution was magnetically stirred for 30 minutes to produce CKGA cryogel. The specific formulation of the synthesized cryogels is detailed in Table 1.

Characterization of Cryogels

The morphologies of the various cryogels were observed using scanning electron microscopy (HITACHI Regulus 8100). The chemical components of the prepared cryogels were characterized by Fourier transform infrared spectroscopy (Nicolet Summit LITE, Thermo Fisher). For the compression test, a cylindrical sample (10 mm diameter, 10 mm height) was compressed at a rate of 5 mm·min^{-1}, and the compressive strength was defined as the stress value when the compressive strain reached 80%. To verify the formation of stable GA/Ag NPs, the mixture of GA and AgNO$_3$ during the cryogel synthesis process was characterized using UV-Vis absorption spectroscopy, and Dynamic Light Scattering (DLS). To determine the swelling ratio of the cryogel, the freeze-dried cryogel was weighed (W$_0$) and then immersed in 100 mL of phosphate-buffered solution (PBS) at 37°C. Once the volume reached equilibrium, the measured mass was recorded as W$_1$. The swelling ratio of the cryogel was calculated using the following formula:

$$\text{Swelling ratio}(\%) = \frac{W_1 - W_0}{W_0} \times 100\%$$

Cell Proliferation and Compatibility Evaluation

CCK-8 assay was employed to evaluate the cell proliferation-promoting ability of CS, CK, and CKGA cryogel samples (Φ=10×1 mm²). Each gel sample was then soaked in DMEM culture medium at a concentration of 1 mg·mL^{-1} for 24 hours to prepare the extract. L929 cells were seeded in a 96-well plate at a density of 5×10³ cells per well and cultured for 6 hours. The medium was then replaced with 100 μL of cryogel extract to continue cell culture. In the control group, 100 μL of DMEM was added. After 24 and 48 hours, cells were washed with PBS and incubated with 100 μL of complete DMEM and 10 μL of CCK-8 reagent for 2 hours. The absorbance at 450 nm (OD$_{450}$) was measured using an enzyme-linked immunosorbent assay reader, and cell viability was calculated using the following formula:

$$\text{Cell viability}(\%) = \frac{\text{ODsample} - \text{ODblank}}{\text{ODcontrol} - \text{ODblank}} \times 100\%$$

To further assess biocompatibility, each group of cryogels was soaked in complete DMEM medium for 24 hours. L929 cells were seeded in 24-well plates at a density of 5×10⁵ cells per well. After 6 hours, 2 mL of complete DMEM was added to the control group. The treatment groups were incubated with 2 mL of DMEM along with the cryogel samples. Two days later, the L929 cells were stained using a live/dead cell staining kit, and cell morphology was observed under a fluorescence microscope.

Table 1 Composition and Proportion of Cryogel

sample	RK31(mg)	CS (mg)	CH$_3$COOH	GA (mM)	AgNO$_3$ (mM)	H$_2$O mL
CS	0	300	200	0	0	10
CK	4	300	200	0	0	10
CKGA1mM	4	300	200	1	1	10
CKGA0.5mM	4	300	200	0.5	0.5	10
CKGA0.25mM	4	300	200	0.25	0.25	10
CKGA0.125mM	4	300	200	0.125	0.125	10

In vitro Antibacterial Test

The antibacterial activity of the cryogel against *S. aureus* and *E. coli* was assessed using the agar diffusion method. A bacterial suspension (10^6 CFU·mL^{-1}) was evenly distributed on LB agar plates. After the bacterial solution dried, the saline-solubilized cryogel samples were gently placed on the bacterial-coated agar surface. After 12 hours of incubation at 37°C, the diameters of the inhibition zones were measured. Additionally, the antibacterial performance was evaluated using the turbidimetric method. Cryogel samples were placed in a 48-well plate, and 200 μL of *S. aureus* or *E. coli* suspension (10^6 CFU·mL^{-1}) was added to the surface of the cryogel. The control group received only 200 μL of bacterial suspension. After 4 hours of incubation, 1 mL of LB broth medium was added to resuspend the bacteria, and incubation continued at 37°C for another 12 hours. The optical density of the culture medium at 600 nm (OD$_{600}$) was measured, and the inhibition rate of the cryogel samples was calculated using the following formula:

$$\text{Antibacterial ratio}\,(\%) = \frac{\text{ODcontrol} - \text{ODsample}}{\text{ODcontrol}} \times 100\%$$

To confirm the antibacterial effects, the spread plate method was employed: 100 μL of bacterial suspension from both treatment and control groups was spread on LB agar plates. After 12 hours of incubation on a shaker, bacterial growth was examined.

Hemolysis Test

Before the experiment, freeze-dried cryogel was soaked in physiological saline and left at 37°C overnight. Then, 1 mL of a 4% rat red blood cell (RBC) suspension was placed into a 1.5 mL centrifuge tube and centrifuged to remove broken RBCs. The RBCs were added to 1 mL of deionized water (positive control), 1 mL of saline with cryogel (experimental group), and 1 mL of saline without cryogel (negative control). After 1 hour of incubation at 37°C, the cryogel was discarded, and the contents were centrifuged at 1000 rpm for 5 minutes. Photographs of each group were taken, and the supernatant's optical density at 540 nm (OD$_{540}$) was measured. The hemolysis rate was calculated using the following formula:

$$\text{Hemolysis}\,(\%) = \frac{\text{ODsample} - \text{ODnegative}}{\text{ODpositive} - \text{ODnegative}} \times 100\%$$

BCI Test and Hemostatic Tests in vivo

The blood clotting index (BCI) was used to evaluate cryogel coagulation performance. Experimental groups included CS, CK, and CKGA cryogel samples, with the control group consisting of gauze blocks of equivalent mass. These materials were placed in a 6-well plate, and 50 μL of calcified blood (CaCl$_2$ concentration of 1×10^{-3} mol·mL^{-1}) was applied to the surface of the cryogel and gauze. After 120 seconds of incubation at 37°C, 5 mL of deionized water was added to wash off non-adherent blood without disrupting the clot. The optical density of the supernatant at 540 nm was measured using a microplate reader to obtain the Is value. A negative reference group was created by mixing 50 μL of blood with 5 mL of physiological saline, with absorbance measured as Ir. The BCI value was calculated using the following formula:

$$\text{BCI}(\%) = \frac{\text{Is}}{\text{Ir}} \times 100\%$$

A rat tail amputation model was used to measure blood loss. Following anesthesia, rats' tails were amputated, and hemostasis was immediately attempted using freeze-dried cryogel. The blank group received no treatment; the control group was treated with gauze; and experimental groups included CS, CK, and CKGA cryogel. Bleeding was observed for 4 minutes, and blood loss was calculated by weighing the filter paper.

ROS Scavenging Assay

The reactive oxygen species (ROS) removal capability of CKGA cryogel was assessed using the Total Antioxidant Capacity (T-AOC) Assay Kits (ABTS and DPPH). CKGA cryogel samples were swelled in 400 μL of deionized water for 12 hours to prepare the extract solution. For the ABTS assay, the working liquid was prepared according to the

instructions. Then, 190 μL of the working liquid was added to a 96-well plate, with 10 μL of deionized water added to the control group and 10 μL of CKGA cryogel extract solution added to the experimental group. The absorbance at 734 nm was measured after 20 minutes of incubation. The ABTS clearance rate was calculated using the following formula:

$$\text{ABTS scavenging ratio}(\%) = \frac{\text{ODcontrol} - \text{ODsample}}{\text{ODcontrol}} \times 100\%$$

For the DPPH assay, 380 μL of DPPH working liquid was added to an EP tube. Then, 20 μL of deionized water was added to the control group and 20 μL of CKGA cryogel extract solution was added to the experimental group. The absorbance at 515 nm was measured after 20 minutes of light-shielded reaction. The DPPH removal rate was calculated using the following formula:

$$\text{DPPH scavenging ratio}(\%) = \frac{\text{ODcontrol} - \text{ODsample}}{\text{ODcontrol}} \times 100\%$$

To evaluate the ROS scavenging efficiency of various cryogels, L929 cells were pretreated with 800 μmol H_2O_2 for 12 hours to induce ROS production. After incubating with different cryogels for 12 hours, the cells were stained with 10 μM DCFH-DA for 30 minutes. The cells were then washed three times with FBS-free medium and photographed using a fluorescent inverted microscope (Olympus, Japan).

In vivo Evaluation of Wound Healing

For the rat model of infected wounds, male SD rats weighing 200–250 g were used as experimental animals. The rats were anesthetized, and their back hair was shaved. An 8-mm diameter full-thickness skin defect was created using a skin punch. A 50 μL of *S. aureus* bacterial solution (10^7 CFU·mL^{-1}) was inoculated at the wound site to induce infection. In the experimental groups, CS, CK, and CKGA cryogels were implanted into the skin wounds and secured with a 3M transparent dressing. In the control group, wounds were covered with an equal mass of gauze and bandaged. On the third day post-operation, wound secretions were collected for culture, and colony counts were performed to assess bacterial load. The wound-healing process was documented with a camera on days 0, 3, 6, 10, and 14 post-operation. After 14 days, the rats were euthanized with an overdose of anesthesia, and skin samples were obtained from the wound site using a skin punch. The samples were fixed in 4% paraformaldehyde, sectioned, and stained with hematoxylin and eosin (H&E) and Masson's trichrome stain. The wound size and stained sections were analyzed using ImageJ software.

Statistical Analysis

All experiments were repeated at least three times, and the experimental data are presented as mean ± standard deviation. Statistical analysis was conducted using one-way or two-way ANOVA with GraphPad Prism 9.4.1. A P value <0.05 was considered statistically significant in all analyses.

Results

Preparation and Characterization of Cryogels

Using natural plant polyphenols as reducing agents for preparing metal nanoparticles aligns with green chemistry principles and offers advantages such as cost-effectiveness, mild synthesis conditions, and simplicity. In this study, GA was utilized as both a reducing and stabilizing agent. Stable silver nanoparticles, referred to as GA/Ag NPs, were formed through the chelation of the two phenolic hydroxyl groups of GA with Ag$^+$. The CK cryogel was soaked in a mixture of GA and AgNO$_3$, and upon adjusting the pH to 11, the solution quickly turned brown, indicating the formation of stable GA/Ag NPs (Figure 1A). A small volume of the GA/Ag NPs solution was used to measure absorbance with a UV-visible spectrophotometer, revealing an absorption peak at 400 nm (Figure 1A), which confirmed the formation of Ag NPs. Transmission electron microscopy (TEM) and dynamic light scattering (DLS) were then employed to characterize the morphology and particle size of the GA/Ag NPs, which appeared as dispersed spherical particles with relatively uniform sizes (Figure 1B–D), and its zeta-potential suggesting that GA/Ag NPs have good water dispersibility and stability (Figure 1C). Due to hydrogen bonding interactions between GA and the CK cryogel, GA/Ag
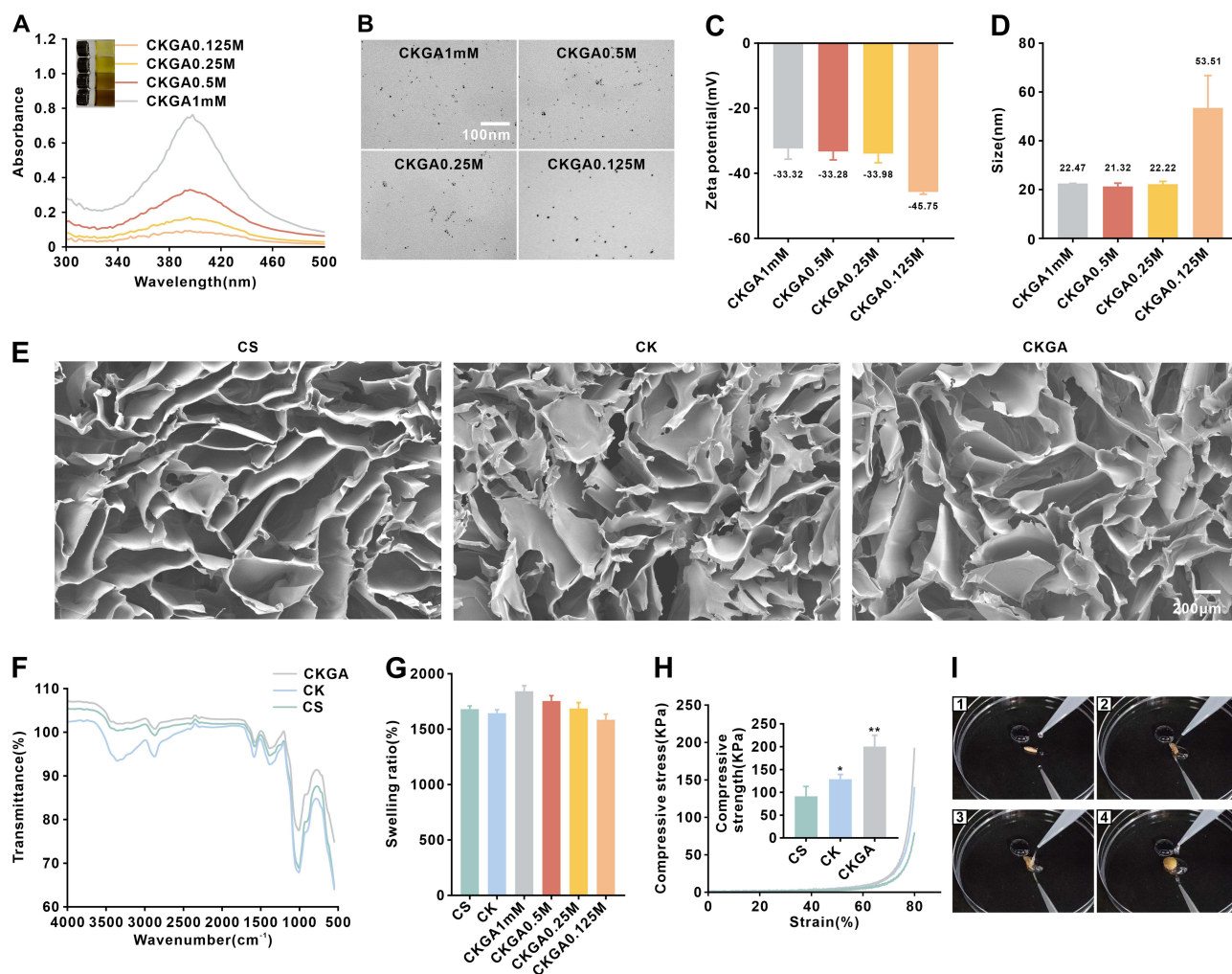
Figure 1 Characterization of cryogels. (**A**) UV–vis spectra of GA/Ag NPs colloid, inserted with photograph of GA/Ag NPs colloid. (**B**) TEM images of GA/Ag NPs. (**C**) Zeta potential data of GA/Ag NPs. (**D**) Dynamic light scattering data of GA/Ag NPs. (**E**) SEM images of various cryogels. (**F**) The FTIR results of various cryogels. (**G**) The swelling ratio (%) of various types of cryogels. (**H**) Typical compression stress–strain curves of various cryogels.*p < 0.05,**p < 0.01. (**I**) A screenshot of the fast water absorption video of CKGA cryogel in 1 seconds. (I1, I2, I3 and I4 screenshot pictures of 0 second, 0.25 second, 0.5 second and 1 second respectively).

NPs were adsorbed into the cryogel, forming the CKGA cryogel. Scanning electron microscopy (SEM) images revealed that all cryogels possess an interpenetrating porous network structure (Figure 1E), beneficial for gas and nutrient exchange, thus promoting cell proliferation and tissue regeneration. The FTIR results are shown in Figure 1F. To simulate the gel's ability to adsorb body fluids during wound healing, the cryogel's swelling properties were measured at pH 7.4 and 37°C, with the CKGA cryogel demonstrating a swelling rate of up to 1800% (Figure 1G). The compressive properties of the various cryogels were also tested (Figure 1H). With increasing strain, the compressive stress increased for all cryogels, and the compressive strength of the CKGA cryogel at 80% compression strain was nearly twice that of the pure CS scaffold. The compressive strength of the CKGA cryogels improved further due to GA forming hydrogen bonds between CS and RK31. To assess recoverability, circle-shaped freeze-dried cryogels were compressed, twisted, and then placed in deionized water. The twisted cryogels returned to their original shape within 1 second upon water absorption, and this recovery process was repeatable (Figure 1I).

Biocompatibility of Cryogels

The cytotoxicity of the cryogels in vitro was assessed using L929 cells and the CCK-8 assay. Due to the favorable biocompatibility of CS and RK31, the cell viability of L929 cells treated with extracts from CS and CK cryogels for 24 hours was slightly higher than that of the control group (Figure 2A). After 48 hours, the CK cryogel group exhibited
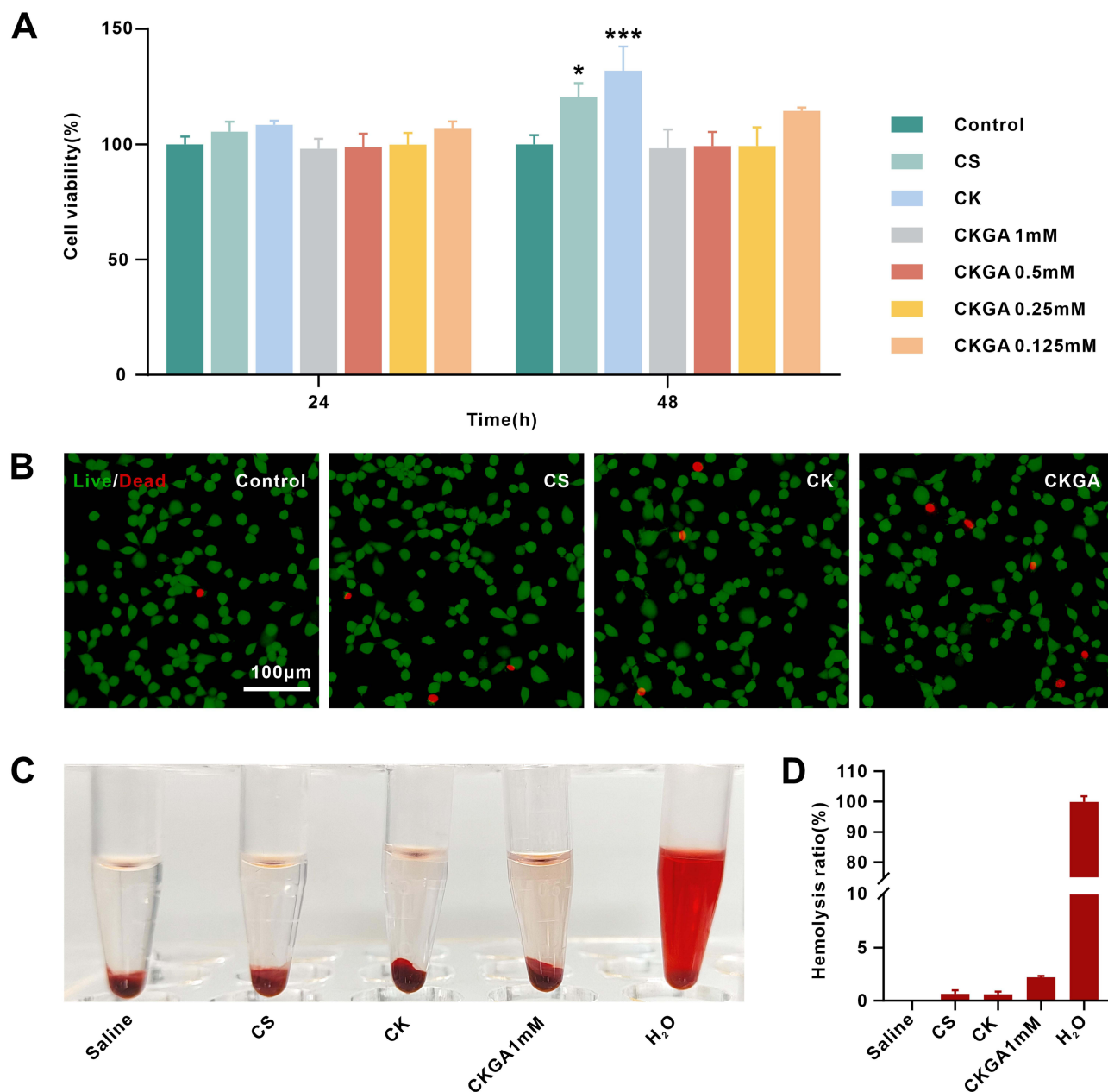
Figure 2 Evaluation of cell proliferation and compatibility of cryogels. (**A**) viability of L929 cells incubated with cryogel extracts for 24 h and 48 h by CCK-8 assay. *p < 0.05, ***p < 0.001. (**B**) The L929 cells were incubated with our cryogels for 48 h before being performed Live-Dead Cell Staining Assay for biocompatibility evaluation. (**C**) Hemolytic photographs of hemolysis assay. (**D**) statistical hemolysis ratios of hemolysis assay. Mean ± SD, n = 3.

the highest cell viability, which may be attributed to the proliferative effect of the added recombinant keratin. None of the CKGA cryogel extracts showed significant cytotoxicity at 24 or 48 hours, with all groups maintaining cell viability above 98%. These results suggest that the CKGA cryogel does not exhibit noticeable cytotoxic effects.

Live/dead cell staining further supported the cryogels' good biocompatibility. After co-incubation with CS, CK, and CKGA cryogels for 48 hours, most cells appeared green, with only a few red dead cells observed. Under high magnification, cells in the cryogel treatment groups were spindle-shaped, similar to those in the control group, indicating that cells maintained good morphology (Figure 2B). The hemolysis assay results showed that the positive control group, exposed to deionized water, exhibited hemolysis and appeared red. In contrast, the supernatants of the CS, CK, and CKGA cryogel groups were almost transparent (Figure 2C). The calculated hemolysis rate ranged from 0.3% to 2.2%,

with no significant difference from the negative control group with saline (Figure 2D). These findings indicate that the cryogels have good blood compatibility and are unlikely to cause hemolysis when applied to bleeding wounds. Overall, the results demonstrate that the CKGA cryogel has excellent biocompatibility and potential for use in wound-dressing applications.

Antibacterial Activity of Cryogels

The antibacterial properties of the cryogel were assessed using an agar diffusion test. The area around the CKGA cryogel was free of bacterial growth, with a distinct inhibition zone, while the CS and CK cryogels, lacking GA/Ag NP modification, showed no inhibition zones (Figure 3A). The size of the inhibition zones increased with higher molar concentrations of GA/Ag NPs in the CKGA cryogel (Figure 3B). The inhibition zone diameter for *E. coli* treated with CKGA cryogel was slightly larger than that for *S. aureus*, suggesting a stronger antibacterial effect against *E. coli*. To
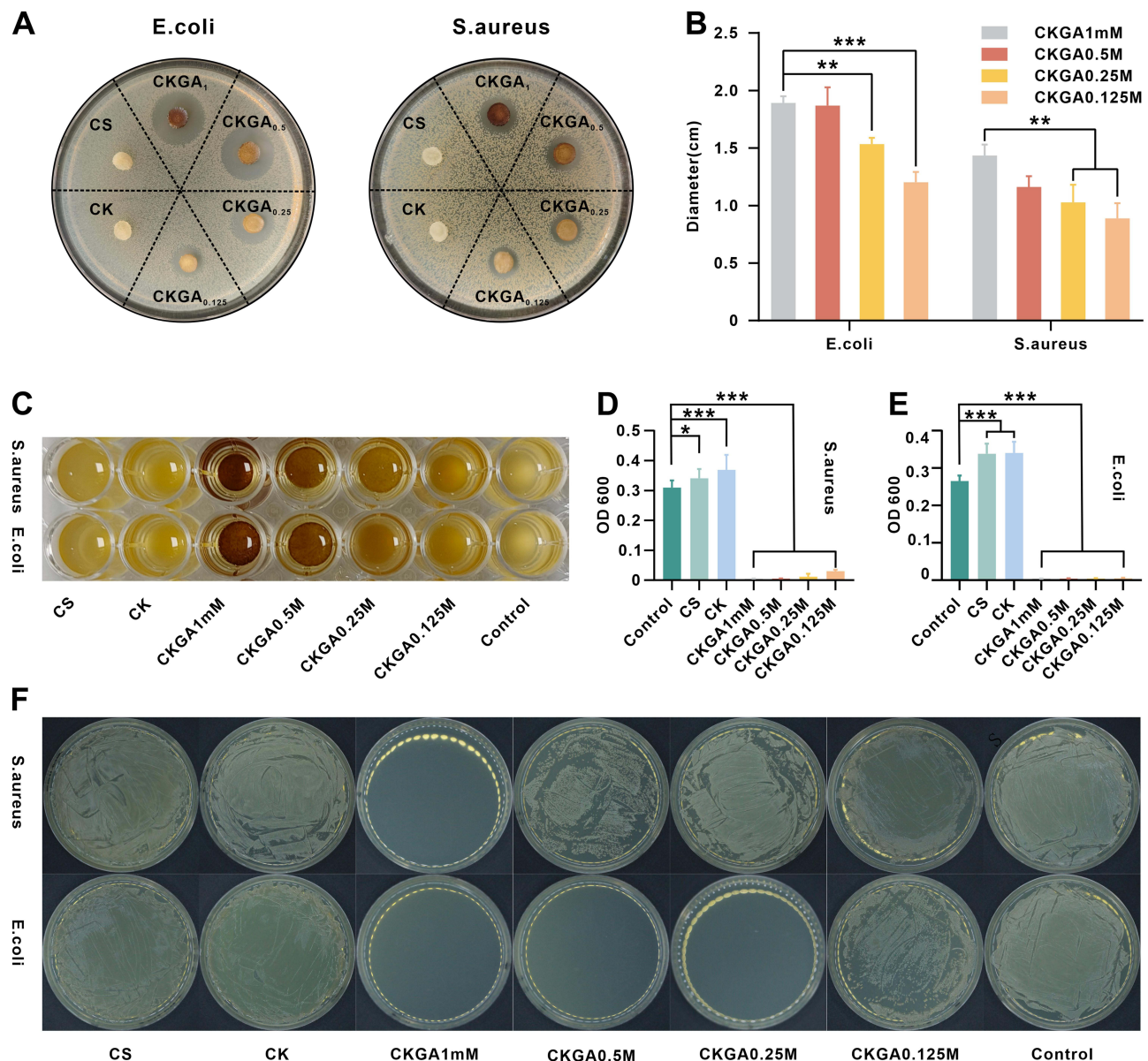

Figure 3 Antibacterial activities of various cryogels in vitro. Photographs (**A**) and diameter (**B**) of inhibition zone against *E. coli* and *S. aureus*. (**C**) Photographs of *S. aureus* and *E. coli* cultured with various cryogels after 16 hours. The OD value of (**D**) *S. aureus* suspension and (**E**) *E. coli* suspension cultured with various cryogels after 16 hours. *p < 0.05, **p < 0.01, ***p < 0.001. Mean ± SD, n = 3. (**F**) Bacterial colonies of the *S. aureus* and *E. coli*.

further examine the antibacterial activity of the CKGA cryogel, *E. coli* and *S. aureus* suspensions were co-incubated with different cryogel groups, followed by resuspension in culture medium for 12 hours. The inhibition rate was then measured using turbidimetry. After 4 hours of co-incubation, the supernatants of the CS, CK, and control groups were significantly murkier than that of the CKGA cryogel group (Figure 3C). The OD_{600} value of the CKGA cryogel was notably lower than that of the other cryogels, achieving an antibacterial rate of 99.9% against both *S. aureus* and *E. coli* at a molar concentration of 0.5–1 mm. The CK cryogel exhibited the highest OD_{600}, potentially due to bacterial contamination after adding RK31 (Figure 3D–E). The bactericidal efficacy of the CKGA cryogel was further confirmed using the spread plate method (Figure 3F). At a molar concentration of 1 mm of GA/Ag NPs, no *S. aureus* colonies were observed on the LB plates, with the antibacterial effect diminishing at lower concentrations. No *E. coli* colonies were seen at GA/Ag NP molar concentrations ranging from 0.25 to 1 mm, indicating that the CKGA cryogel had a stronger inhibitory effect against *E. coli*, consistent with the zone of inhibition results. These findings suggest that the CKGA cryogel can achieve a 99.9% inhibition rate against both *S. aureus* and *E. coli* at a GA/Ag NP molar concentration of 1 mm and has a stronger antibacterial effect against *E. coli* compared to *S. aureus*.

Hemostatic Evaluation of Cryogels

BCI is a crucial parameter for evaluating the hemostatic properties of materials, with a higher BCI value indicating poorer hemostatic ability.[14] Compared with gauze, the CS, CK, and CKGA cryogels had lower BCI values, with the CKGA cryogel showing a BCI of less than 10%, reflecting its excellent hemostatic effects (Figure 4A). The in vivo hemostatic action of various cryogels was evaluated using a rat tail amputation model (Figure 4B). The control and gauze groups experienced significantly higher blood loss than the cryogel groups (Figure 4C). Within 4 minutes, the control and gauze groups exhibited more bleeding, while bleeding was significantly reduced in the CS, CK, and CKGA cryogel-treated groups (Figure 4D). SEM imaging revealed RBC adhesion and morphology on the gauze and cryogels (Figure 4E). A large number of RBCs adhered to the porous structure of the CS, CK, and CKGA cryogels, whereas only a few adhered to the gauze. RBCs on the CS cryogel appeared spherical, likely due to chitosan's positively charged cationic polysaccharide.[28] On the CK and CKGA cryogels, most RBCs were biconcave discs, suggesting good cytocompatibility and blood adhesive properties, highlighting their potential for hemostatic applications.

Antioxidant Performance of CKGA Cryogels

Excessive production and accumulation of free radicals at the wound site can cause oxidative stress, leading to cellular dysfunction or apoptosis and affecting wound healing. GA, a natural polyphenol, has a high capacity for scavenging reactive oxygen species across a wide range of free radicals. In this study, we investigated the antioxidant activity of CKGA cryogel by examining its ability to scavenge ABTS and DPPH in vitro, as well as its ability to protect cells from H_2O_2 damage. The scavenging ability of CKGA cryogel against hydroxyl and nitrogen radicals is shown in the Figure 5. The color of the ABTS and DPPH working solutions became lighter after treatment with the CKGA cryogel extract (Figure 5A and B). The highest scavenging rate was observed at 1 mm of CKGA, with a decrease in scavenging as the concentration lowered (Figure 5C and D). Additionally, DCFH-DA staining was used to evaluate the antioxidant protective effect of the cryogel on H_2O_2-stimulated L929 cells. As depicted in the figure, strong green fluorescence was visible in the H_2O_2 group after incubation with 800 μmol H_2O_2 for 12 hours, indicating substantial ROS production in the cells. However, the fluorescence intensity in the cryogel group was significantly reduced ($p<0.001$), indicating that CKGA cryogel effectively scavenged intracellular ROS and exhibited antioxidant protective effects.

Wound Healing Effect

A rat wound infection model was employed to assess the ability of each cryogel group to promote wound healing. On the third day post-surgery, wound exudate was cultured and spread on LB agar plate. As shown in Figure 6A, the CKGA cryogel-treated group had the lowest number of bacterial colonies on the wound, while the other groups had a considerable number of colonies. Photographs were taken, and the wound healing rate was analyzed using ImageJ software, as illustrated in Figure 6B. Throughout the healing process, CKGA cryogel demonstrated the best therapeutic effect. On day 14, the wounds in the CKGA cryogel-treated group showed no obvious skin defects, while scabs remained
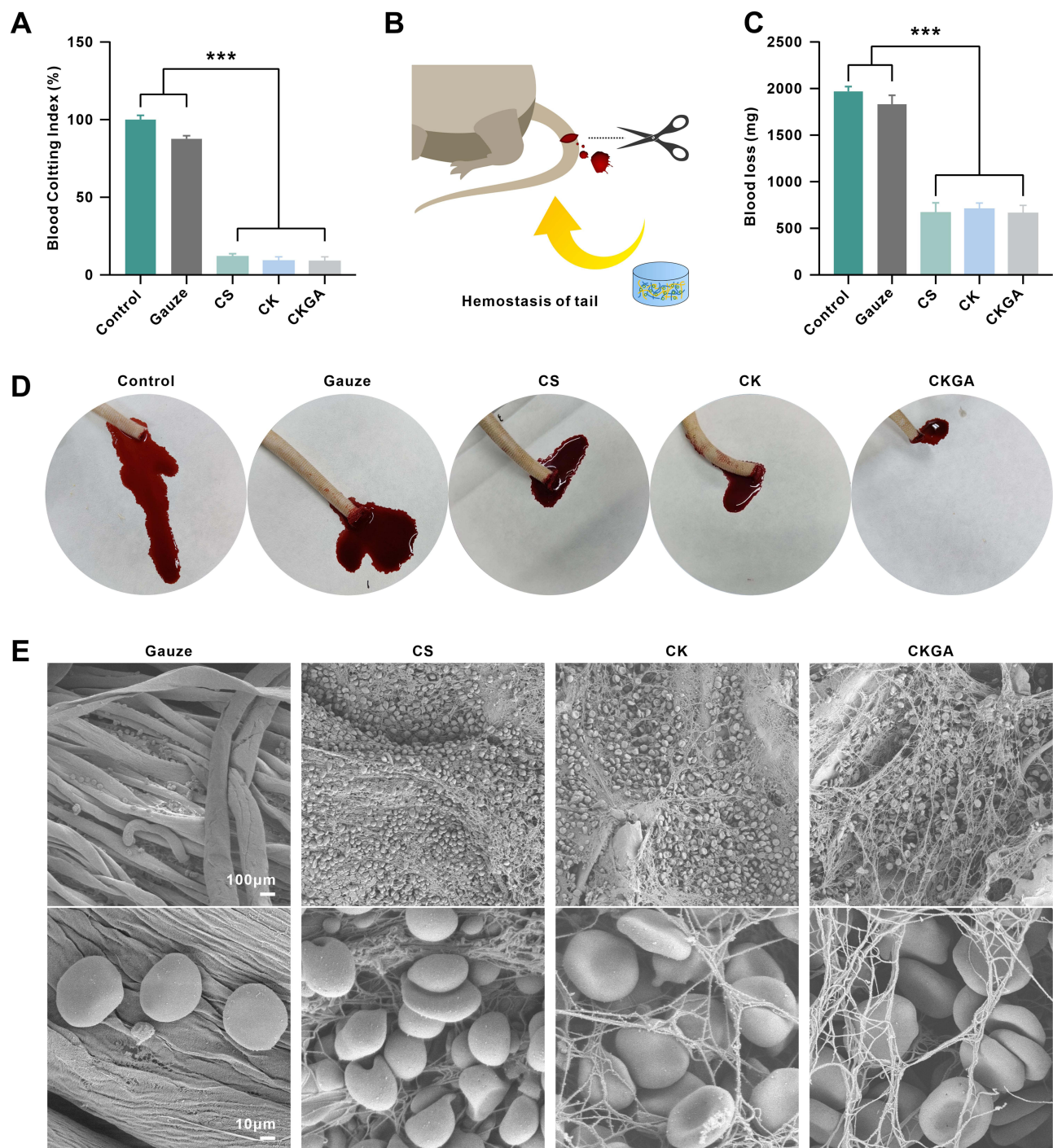
Figure 4 Hemostatic evaluation of cryogels. (**A**) Statistical analysis of Blood Clotting Index (BCI) of cryogels and Gauze. ***p < 0.001.Mean ± SD, n = 3. (**B**) Schematic diagram of tail amputation model. (**C**) Statistics of blood loss of tail amputation model without treatment (Control), with Gauze or cryogels treatments. ***p < 0.001.Mean ± SD, n = 3. (**D**) Photographs of blood trace. (**E**) SEM images of hemocyte adhesion on Gauze, CS, CK and CKGA cryogels.

in the other groups. Figure 6C shows that on days 6, 10, and 14, the wound healing rate of the CKGA cryogel group was higher than that of the other groups, with nearly 96% healing at day 14 compared to approximately 80% for the control, CS, and CK cryogel groups. Tissue samples from the healed wound areas were taken for H&E staining to observe tissue regeneration. As shown in Figure 6D, wounds treated with CKGA cryogel exhibited less inflammatory cell infiltration and mature granulation tissue with increased neovascularization. In contrast, wounds in the control group and those treated with CS and CK cryogels displayed immature granulation tissue with heavy inflammatory cell infiltration,
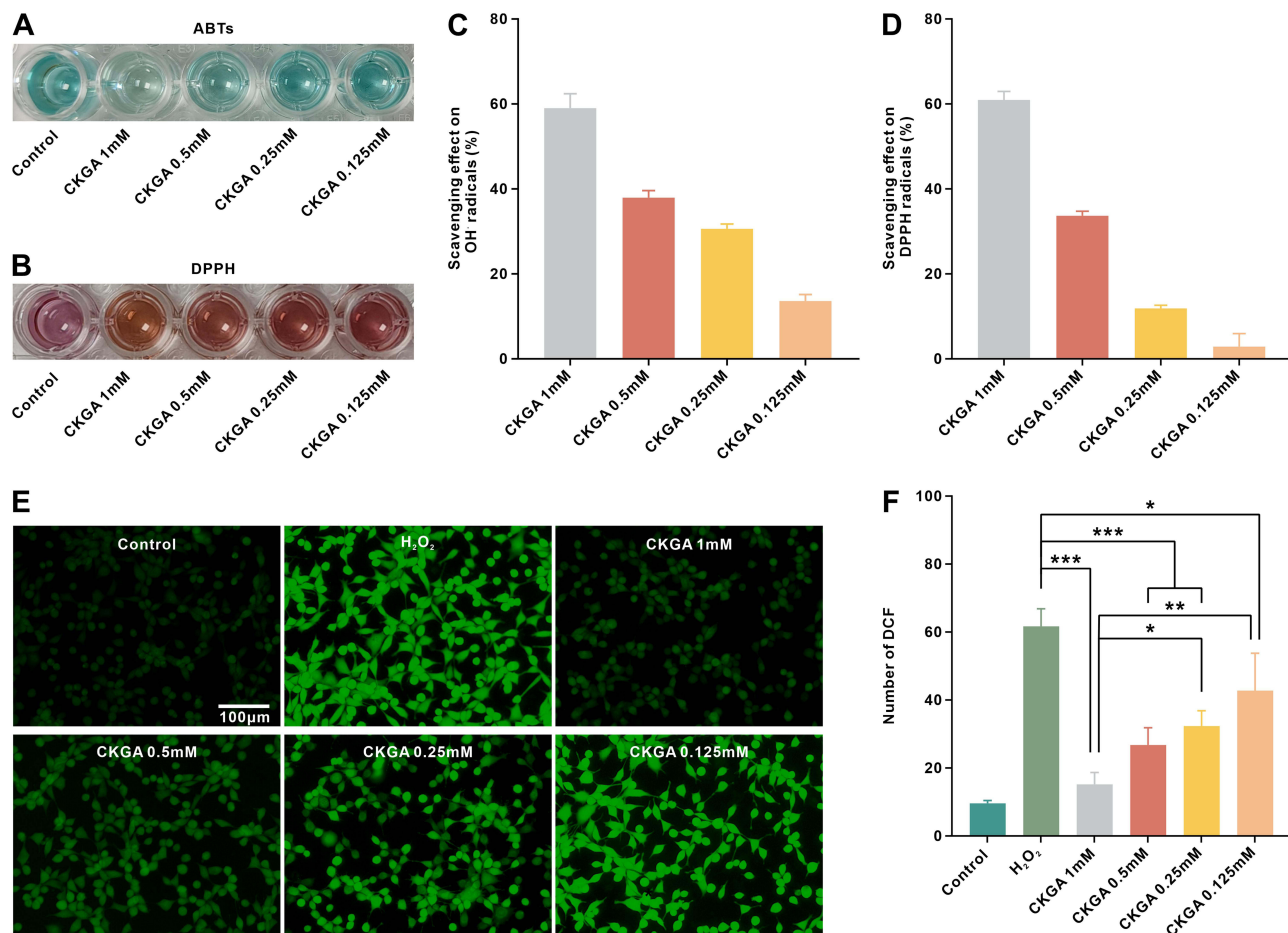
Figure 5 Antioxidant performance of CKGA cryogels. Photographs of ABTS assay (**A**) and DPPH assay (**B**). Scavenging ratio against (**C**) hydroxylic radicals and (**D**) DPPH free radicals. Fluorescence staining images of L929 cells treated without H_2O_2 (Control group), with 800 μM H_2O_2 (H_2O_2 group), 800 μM H_2O_2 and CKGA 1mM (CKGA 1mM), 800 μM H_2O_2 and CKGA 0.5mM (CKGA1mM), 800 μM H_2O_2 and CKGA 0.25mM (CKGA 0.25mM), 800 μM H_2O_2 and CKGA 0.125mM (CKGA0.125mM). (**F**) statistical analysis of fluorescence intensity of DCF. *$p < 0.05$, **$p < 0.01$,***$p < 0.001$. Mean ± SD, n = 3.

indicating incomplete healing. Masson's trichrome staining results showed that the CKGA group had more mature and closely aligned collagen fibers compared to the other groups, suggesting improved extracellular matrix and tissue remodeling. To verify the tissue toxicity of the cryogels, tissue samples from major organs of the rats were acquired and stained with H&E (Figure 6E). No significant differences were observed between the organs of rats treated with CKGA cryogel and those of normal rats, indicating that the cryogels did not exhibit apparent tissue toxicity.

Discussion

An ideal dressing should have the ability to absorb exudate, prevent infection, maintain moisture and breathability, act as a barrier to harmful substances, and promote tissue repair.[29] Cryogels, with their three-dimensional network structure, create a favorable environment for cell adhesion and growth. They can also incorporate drugs, polymers, and various metal ions, endowing them with specific physicochemical properties and functions. This makes cryogels promising materials for wound dressings. Cryogels made from chitosan (CS) form an interpenetrating porous network, which provides excellent swelling properties and hemostatic efficacy. In this study, the CKGA cryogel synthesized with CS as the primary matrix demonstrated a swelling ratio of up to 1800%, effectively absorbing exudate and maintaining a moist and breathable environment for wound healing. Additionally, this cryogel exhibited good elasticity, recoverability, and resistance to pulling, fitting snugly against the wound and promoting effective healing.

In this study, a cryogel was prepared by blending RK31 with CS, enhancing the bioactivity of the CS cryogel while leveraging CS's favorable physical properties to address the poor mechanical performance of RK31. This expands the
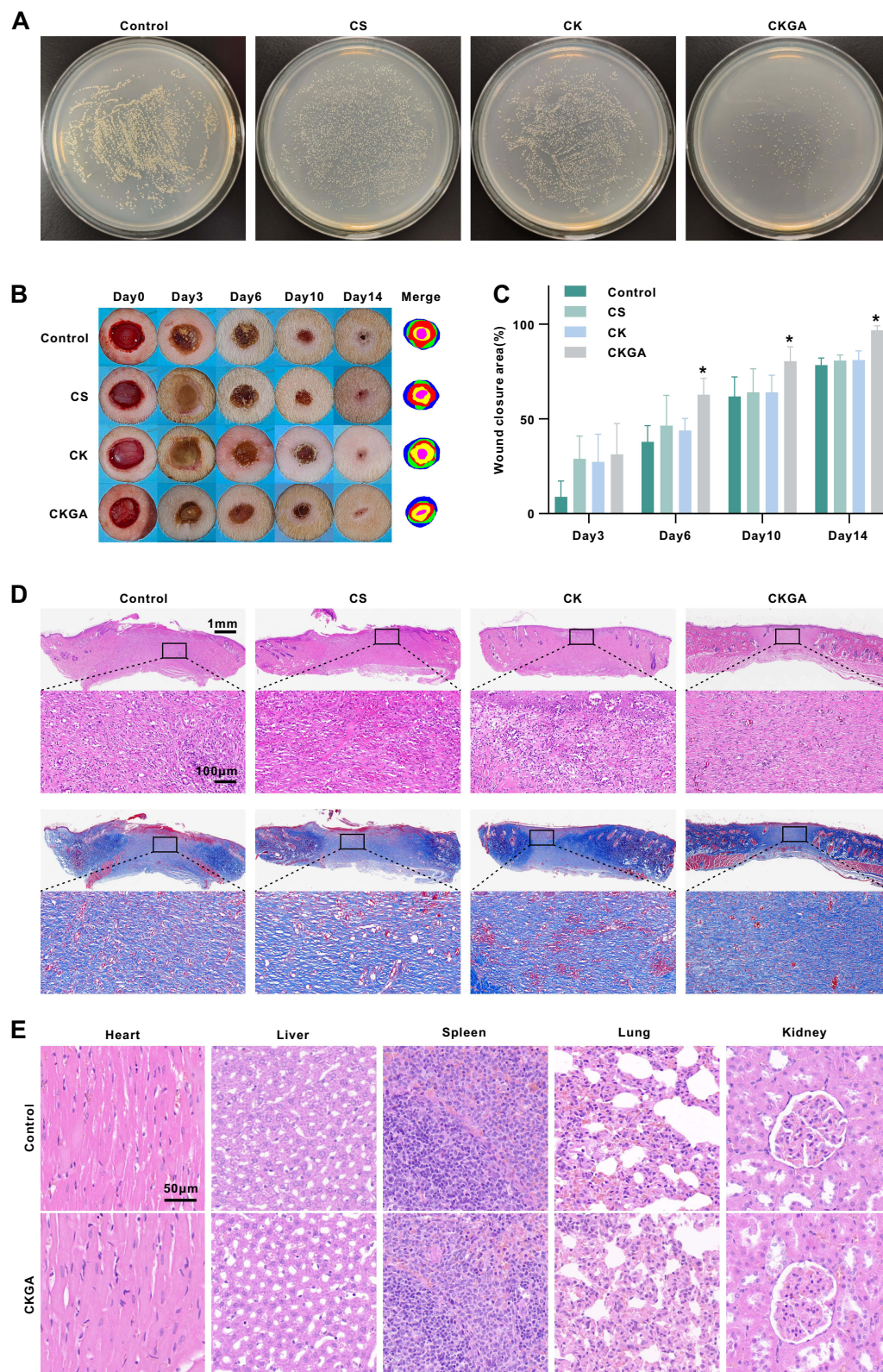
Figure 6 In vivo *S. aureus* infection wound healing assessment of various cryogels.(**A**) Bacterial colonies of the pus of wound site after treatment for 3 days. (**B**) Photographs of the wounds accompanied by an infection with S. aureus following control, CS, CK and CKGA cryogels treatment. (**C**) The wound healing ratio with various treatments after different healing periods. *p < 0.05. Mean ± SD, n = 5. (**D**) H&E and Masson's trichrome stain of the wound section on the 14th day. (**E**) Visceral toxicity after CKGA cryogel treatment of damaged skin.

range of RK31's applications. Both CS and RK31 are low-immunogenic materials, making the synthesized cryogel safe for wound application.[30,31] However, CK cryogels lack inherent antimicrobial properties and are susceptible to bacterial contamination. CS cryogels achieve significant antibacterial efficacy only when loaded with other antibacterial components. Incorporating silver nanoparticles (AgNPs) addresses this issue but poses potential risks related to their low safety concentration.[32] Biocompatibility was evaluated through cell culture with extracts from each cryogel group to assess cytotoxicity and proliferation-promoting effects on L929 cells. The cryogels were also co-cultured with L929 cells, followed by live/dead cell staining to observe cell morphology. Results indicated that the CK cryogel had a stronger cell proliferation-promoting effect compared to the CS cryogel, suggesting that recombinant keratin enhances the bioactivity of the CS cryogel. The CKGA cryogel containing GA/AgNPs showed no significant differences in cell vitality and live/dead staining compared to the control group. The hemolysis rate, as indicated by the hemolysis test, was below 5%, meeting the biocompatibility requirements for medical materials.[33] This low rate is due to the excellent dispersibility of GA-reduced Ag NPs and the formation of a protective layer from GA adsorption on the Ag NP surface. The reaction process is mild and does not involve toxic or harmful catalysts, contributing to the biocompatibility of CKGA cryogels.

CS is a positively charged alkaline polysaccharide that interacts electrostatically with cell membrane groups to promote cell aggregation. Additionally, the porous structure of the CS cryogel supports RBC and platelet adherence, enhancing its hemostatic properties.[34] Studies have shown that chitosan sponges modified with natural polyphenols exhibit good hydrophilicity and are effective for hemostasis in superficial wounds.[35–37] In a rat tail amputation model, the bleeding amount in the cryogel group was lower compared to the control and blank groups. This improvement is due to the enhanced hemostatic properties of CK cryogels functionalized with RK31. Electron microscopy revealed that RBCs maintained good morphology when adhering to CK cryogels, whereas CS cryogels led to abnormal RBC morphology due to their positive charge. Furthermore, plasma proteins, rich in amines and amino groups, can form covalent bonds with the oxidized GA phenolic hydroxyl groups in CKGA cryogels, promoting blood clot formation and hemostatic effects.[38,39]

Bacterial infection must be considered during wound treatment, as prolonged infections can lead to chronic inflammation and impair wound healing. Dressings with antibacterial properties help reduce bacterial load, inhibit biofilm formation, and accelerate healing.[40,41] The CKGA cryogel, supplemented with GA/Ag NPs, demonstrated excellent antibacterial efficacy. In vitro tests showed that at a concentration of 1 mm GA/Ag NPs, the cryogel achieved a 99.9% antibacterial rate against both *E. coli* and *S. aureus*. Ag NPs provide broad-spectrum antibacterial effects, targeting various bacteria, fungi, viruses, and some drug-resistant strains. The study found that CKGA cryogels were particularly effective against *E. coli*, possibly due to E. coli's thinner cell wall, which allows easier penetration and interaction of GA/Ag NPs, disrupting cell wall integrity and killing the bacteria.[42] The CKGA cryogel demonstrated effective antibacterial activity in a rat wound infection model. On the third day post-surgery, less purulent exudate was observed in the CKGA cryogel group compared to the control, CS, and CK cryogel groups when the dressing was removed. Wound secretions treated with CKGA cryogel culture showed fewer colonies upon plate spreading, while the control, CS, and CK cryogel groups did not effectively inhibit bacterial proliferation. H&E staining and Masson's trichrome staining results indicated that CKGA cryogel could alleviate the inflammatory response and promote wound healing. The CKGA cryogel enhances wound healing through several mechanisms: Firstly, the CS cryogel isolates contamination, protects the wound, and promotes blood clotting. CS-based cryogels regulate cytokine release during the inflammatory phase, creating a conducive microenvironment for healing.[43,44] They also stimulate fibroblast proliferation and promote collagen deposition. Additionally, recombinant keratin, with its higher purity and stronger biological effects compared to extracted keratin, combined with growth factor (bFGF) in a gel, was shown to enhance cell proliferation, migration, angiogenesis, local collagen deposition, and epithelial mesenchyme transformation in diabetic rat models, accelerating wound healing.[45] Thus, the inclusion of RK31 in CKGA cryogel further boosts its biological activity across all stages of wound healing. Secondly, the GA/Ag NPs in the cryogel effectively inhibit bacterial growth, preventing infection and reducing local tissue inflammation. Studies have shown that GA-based hydrogels, used for treating gastric and skin wounds, regulate oxidative stress, inhibit apoptosis, and possess anti-inflammatory properties.[46,47] The GA/Ag NPs in CKGA cryogels retain unoxidized phenolic hydroxyls with strong antioxidant properties, which help scavenge ROS in the wound environment, shorten the inflammation period, and promote healing.

Conclusion

By using CS and RK31 as a cryogel matrix, the CKGA was successfully prepared with in situ reduction of GA/Ag NPs as an active antibacterial component. The CKGA cryogel exhibited good mechanical properties and biocompatibility, effectively absorbing exudates and achieving rapid hemostasis. The incorporation of GA/Ag NPs endowed the cryogel with significant antioxidant and antibacterial properties, enabling it to scavenge ROS and inhibit bacterial proliferation. In SD rat models with infected wounds, CKGA showed superior wound healing by promoting epidermal regeneration and collagen deposition. These results suggest promising potential for CKGA in treating infected wounds.

Abbreviations

CS, Chitosan; RK31, CK, Recombinant keratin 31; CS/RK31 cryogel; CKGA, CS/K31@GA/Ag cryogel; GA/Ag NPs, Gallic acid-reduced silver nanoparticles; SEM, scanning electron microscopy; TEM, transmission electron microscopy; DPPH,1.1-diphenyl-2-trinitrophenylhydrazine; ROS, Reactive oxygen species; BCI, Blood clotting index.

Ethics Approval and Informed Consent

All animal experimental procedures were approved by the Army Medical University Animal Ethics Committee, ensuring that the care and use of animals conformed to the National Institutes of Health guide for the care and use of laboratory animals (AMUWEC20245212; Approval Date: 2024-3-9).

Consent for Publication

The authors declare that they have no known competing financial interests or personal relationships that could have appeared to influence the work reported in this paper.

Acknowledgments

Author Contributions

All authors made a significant contribution to the work reported, whether that is in the conception, study design, execution, acquisition of data, analysis and interpretation, or in all these areas; took part in drafting, revising or critically reviewing the article; gave final approval of the version to be published; have agreed on the journal to which the article has been submitted; and agree to be accountable for all aspects of the work.

Funding

Disclosure

The authors report no conflicts of interest in this work.

References

1. Sen CK. Human wound and its burden: updated 2020 compendium of estimates. *Adv Wound Care*. 2021;10:281–292. doi:10.1089/wound.2021.0026
2. Hu Q, Nie Y, Xiang J, et al. Injectable sodium alginate hydrogel loaded with plant polyphenol-functionalized silver nanoparticles for bacteria-infected wound healing. *Int J Biol Macromol*. 2023;234:123691. doi:10.1016/j.ijbiomac.2023.123691
3. Sanjarnia P, Picchio ML, Polegre Solis AN, et al. Bringing innovative wound care polymer materials to the market: challenges, developments, and new trends. *Adv Drug Deliv Rev*. 2024;207:115217. doi:10.1016/j.addr.2024.115217
4. Wang Y, Yang Y, Shi Y, Song H, Yu C. Antibiotic-free antibacterial strategies enabled by nanomaterials: progress and perspectives. *Adv Mater*. 2020;32:e1904106. doi:10.1002/adma.201904106
5. He X, Lv Y, Lin Y, et al. Platinum nanoparticles regulated VC MXene nanoplatforms with NIR-II enhanced nanozyme effect for photothermal and chemodynamic anti-infective therapy. *Adv Mater*. 2024;36:e2400366. doi:10.1002/adma.202400366
6. He X, Dai L, Ye L, et al. A vehicle-free antimicrobial polymer hybrid gold nanoparticle as synergistically therapeutic platforms for Staphylococcus aureus infected wound healing. *Adv Sci*. 2022;9:e2105223. doi:10.1002/advs.202105223

7. He X, Hou J-T, Sun X, et al. NIR-II photo-amplified sonodynamic therapy using sodium molybdenum bronze nanoplatform against subcutaneous Staphylococcus aureus infection. *Adv Funct Mater*. 2022;32. doi:10.1002/adfm.202203964

8. He X, Qian Y, Wu C, et al. Entropy-mediated high-entropy MXenes nanotherapeutics: NIR-II-enhanced intrinsic oxidase mimic activity to combat methicillin-resistant Staphylococcus aureus infection. *Adv Mater*. 2023;35:e2211432. doi:10.1002/adma.202211432

9. Verma ML, Dhanya BS, Sukriti, et al. Carbohydrate and protein based biopolymeric nanoparticles: current status and biotechnological applications. *Int J Biol Macromol*. 2020;154:390–412. doi:10.1016/j.ijbiomac.2020.03.105

10. Ye W, Qin M, Qiu R, Li J. Keratin-based wound dressings: from waste to wealth. *Int J Biol Macromol*. 2022;211:183–197. doi:10.1016/j.ijbiomac.2022.04.216

11. Gao F, Li W, Deng J, et al. Recombinant human hair keratin nanoparticles accelerate dermal wound healing. *ACS Appl Mater Interfaces*. 2019;11:18681–18690. doi:10.1021/acsami.9b01725

12. Shariatinia Z. Pharmaceutical applications of chitosan. *Adv Colloid Interface Sci*. 2019;263:131–194. doi:10.1016/j.cis.2018.11.008

13. Yan -R-R, Xue D, Su C, et al. A keratin/chitosan sponge with excellent hemostatic performance for uncontrolled bleeding. *Colloids Surf B Biointerfaces*. 2022;218:112770. doi:10.1016/j.colsurfb.2022.112770

14. Xu N, Yuan Y, Ding L, et al. Multifunctional chitosan/gelatin@tannic acid cryogels decorated with in situ reduced silver nanoparticles for wound healing. *Burns Trauma*. 2022;10:tkac019. doi:10.1093/burnst/tkac019

15. Jia B, Li G, Cao E, Luo J, Zhao X, Huang H. Recent progress of antibacterial hydrogels in wound dressings. *Mater Today Bio*. 2023;19:100582. doi:10.1016/j.mtbio.2023.100582

16. Wu J, Zheng Y, Song W, et al. In situ synthesis of silver-nanoparticles/bacterial cellulose composites for slow-released antimicrobial wound dressing. *Carbohydr Polym*. 2014;102:762–771. doi:10.1016/j.carbpol.2013.10.093

17. Choi JE, Kim S, Ahn JH, et al. Induction of oxidative stress and apoptosis by silver nanoparticles in the liver of adult zebrafish. *Aquat Toxicol*. 2010;100:151–159. doi:10.1016/j.aquatox.2009.12.012

18. Strużyńska L. Dual implications of nanosilver-induced autophagy: nanotoxicity and anti-cancer effects. *Int J Mol Sci*. 2023;24. doi:10.3390/ijms242015386

19. Fageria L, Bambroo V, Mathew A, Mukherjee S, Chowdhury R, Pande S. Functional autophagic flux regulates AgNP uptake and the internalized nanoparticles determine tumor cell fate by temporally regulating flux. *Int J Nanomed*. 2019;14:9063–9076. doi:10.2147/IJN.S222211

20. Chen L, Wu M, Jiang S, et al. Skin toxicity assessment of silver nanoparticles in a 3D epidermal model compared to 2D keratinocytes. *Int J Nanomed*. 2019;14:9707–9719. doi:10.2147/IJN.S225451

21. Trop M, Novak M, Rodl S, Hellbom B, Kroell W, Goessler W. Silver-coated dressing acticoat caused raised liver enzymes and argyria-like symptoms in burn patient. *J Trauma*. 2006;60:648–652. doi:10.1097/01.ta.0000208126.22089.b6

22. Wang X-Q, Chang H-E, Francis R, et al. Silver deposits in cutaneous burn scar tissue is a common phenomenon following application of a silver dressing. *J Cutan Pathol*. 2009;36:788–792. doi:10.1111/j.1600-0560.2008.01141.x

23. Kittler S, Greulich C, Diendorf J, Köller M, Epple M. Toxicity of silver nanoparticles increases during storage because of slow dissolution under release of silver ions. *Chem Mater*. 2010;22:4548–4554. doi:10.1021/cm100023p

24. Hernández-Díaz JA, Garza-García JJ, Zamudio-Ojeda A, León-Morales JM, López-Velázquez JC, García-Morales S. Plant-mediated synthesis of nanoparticles and their antimicrobial activity against phytopathogens. *J Sci Food Agric*. 2021;101:1270–1287. doi:10.1002/jsfa.10767

25. Weian W, Yunxin Y, Ziyan W, Qianzhou J, Lvhua G. Gallic acid: design of a pyrogallol-containing hydrogel and its biomedical applications. *Biomater Sci*. 2024;12:1405–1424. doi:10.1039/d3bm01925j

26. Martínez-Castañón GA, Niño-Martínez N, Martínez-Gutierrez F, Martínez-Mendoza JR, Ruiz F. Synthesis and antibacterial activity of silver nanoparticles with different sizes. *J Nanopart Res*. 2008;10:1343–1348. doi:10.1007/s11051-008-9428-6

27. Liu G, Haiqi G, Li K, Xiang J, Lan T, Zhang Z. Fabrication of silver nanoparticle sponge leather with durable antibacterial property. *J Colloid Interface Sci*. 2018;514:338–348. doi:10.1016/j.jcis.2017.09.049

28. Liu Z, Xu Y, Su H, et al. Chitosan-based hemostatic sponges as new generation hemostatic materials for uncontrolled bleeding emergency: modification, composition, and applications. *Carbohydr Polym*. 2023;311:120780. doi:10.1016/j.carbpol.2023.120780

29. Ali Zahid A, Chakraborty A, Shamiya Y, Ravi SP, Paul A. Leveraging the advancements in functional biomaterials and scaffold fabrication technologies for chronic wound healing applications. *Mater Horiz*. 2022;9:1850–1865. doi:10.1039/d2mh00115b

30. Ali A, Ahmed S. A review on chitosan and its nanocomposites in drug delivery. *Int J Biol Macromol*. 2018;109:273–286. doi:10.1016/j.ijbiomac.2017.12.078

31. Feroz S, Muhammad N, Ranayake J, Dias GK. Based materials for biomedical applications. *Bioact Mater*. 2020;5:496–509. doi:10.1016/j.bioactmat.2020.04.007

32. Gong X, Jadhav ND, Lonikar VV, et al. An overview of green synthesized silver nanoparticles towards bioactive antibacterial, antimicrobial and antifungal applications. *Adv Colloid Interface Sci*. 2024;323:103053. doi:10.1016/j.cis.2023.103053

33. Chang R, Zhao D, Zhang C, et al. Nanocomposite multifunctional hyaluronic acid hydrogel with photothermal antibacterial and antioxidant properties for infected wound healing. *Int J Biol Macromol*. 2023;226:870–884. doi:10.1016/j.ijbiomac.2022.12.116

34. Khan MA, Mujahid M. A review on recent advances in chitosan based composite for hemostatic dressings. *Int J Biol Macromol*. 2019;124:138–147. doi:10.1016/j.ijbiomac.2018.11.045

35. Hu Q, Luo Y. Polyphenol-chitosan conjugates: synthesis, characterization, and applications. *Carbohydr Polym*. 2016;151:624–639. doi:10.1016/j.carbpol.2016.05.109

36. Ren Z, Li M, Wang F, Qiao J, Kaya MGA, Tang K. Antibacterial chitosan-based composite sponge with synergistic hemostatic effect for massive haemorrhage. *Int J Biol Macromol*. 2023;252:126344. doi:10.1016/j.ijbiomac.2023.126344

37. Sun C, Zeng X, Zheng S, et al. Bio-adhesive catechol-modified chitosan wound healing hydrogel dressings through glow discharge plasma technique. *Chem Eng J*. 2022;427:130843. doi:10.1016/j.cej.2021.130843

38. Ryu JH, Choi JS, Park E, et al. Chitosan oral patches inspired by mussel adhesion. *J Control Release*. 2020;317:57–66. doi:10.1016/j.jconrel.2019.11.006

39. Saiz-Poseu J, Mancebo-Aracil J, Nador F, Busqué F, Ruiz-Molina D. The chemistry behind catechol-based adhesion. *Angew Chem Int Ed Engl*. 2019;58:696–714. doi:10.1002/anie.201801063

40. Eggermont LJ, Rogers ZJ, Colombani T, Memic A, Bencherif SA. Injectable cryogels for biomedical applications. *Trends Biotechnol*. 2020;38:418–431. doi:10.1016/j.tibtech.2019.09.008

41. Akin B, Ozmen MM. Antimicrobial cryogel dressings towards effective wound healing. *Prog Biomater*. 2022;11:331–346. doi:10.1007/s40204-022-00202-w

42. Nemčeková K, Svitková V, Sochr J, Gemeiner P, Labuda J. Gallic acid-coated silver nanoparticles as perspective drug nanocarriers: bioanalytical study. *Anal Bioanal Chem*. 2022;414:5493–5505. doi:10.1007/s00216-022-03955-2

43. Liu H, Wang C, Li C, et al. A functional chitosan-based hydrogel as a wound dressing and drug delivery system in the treatment of wound healing. *RSC Adv*. 2018;8:7533–7549. doi:10.1039/c7ra13510f

44. Wang Y, Wang Z, Lu W, Hu Y. Review on chitosan-based antibacterial hydrogels: preparation, mechanisms, and applications. *Int J Biol Macromol*. 2024;255:128080. doi:10.1016/j.ijbiomac.2023.128080

45. Sun C, Huang Y, Wang L, et al. Engineered keratin/bFGF hydrogel to promote diabetic wound healing in rats. *Int J Biol Macromol*. 2024;261:129725. doi:10.1016/j.ijbiomac.2024.129725

46. Huang H, Gong W, Wang X, He W, Hou Y, Hu J. Self-assembly of naturally small molecules into supramolecular fibrillar networks for wound healing. *Adv Healthc Mater*. 2022;11:e2102476. doi:10.1002/adhm.202102476

47. Huang H, Hou Y, Chen L, et al. Multifunctional gallic acid self-assembled hydrogel for alleviation of ethanol-induced acute gastric injury. *Int J Pharm*. 2023;645:123372. doi:10.1016/j.ijpharm.2023.123372